Rapid Communications

Quantum-enhanced sensing from hyperentanglement

S. P. Walborn, A. H. Pimentel, L. Davidovich, and R. L. de Matos Filho
Instituto de Física, Universidade Federal do Rio de Janeiro, P.O. Box 68528, Rio de Janeiro, RJ 21941-972, Brazil

(Received 31 July 2017; published 12 January 2018)

Hyperentanglement—simultaneous entanglement between multiple degrees of freedom of two or more systems—has been used to enhance quantum information tasks such as quantum communication and photonic quantum computing. Here we show that hyperentanglement can lead to increased quantum advantage in metrology, with contributions from the entanglement in each degree of freedom, allowing for Heisenberg scaling in the precision of parameter estimation. Our experiment employs photon pairs entangled in polarization and spatial degrees of freedom to estimate a small tilt angle of a mirror. Precision limits beyond shot noise are saturated through a simple binary measurement of the polarization state. The dynamics considered here have broad applicability, implying that similar strategies based on hyperentanglement can offer improvement in a wide variety of physical scenarios and metrological tasks.

DOI: 10.1103/PhysRevA.97.010301

Introduction. To exploit the advantage of quantum entanglement, for tasks such as computation and metrology, requires producing high-dimensional quantum states composed of many entangled subsystems [1–4]. In addition to the difficulty in producing large entangled states, they are typically very sensitive to noise [5–7]. An alternative route to enhance the size of a system is through hyperentanglement [8], that is, taking advantage of the entanglement in multiple degrees of freedom (DOF) of a composite quantum system. So far, hyperentanglement has found limited use, with a few applications in high-capacity quantum communication [9–13], photonic quantum computing [14,15], tests of quantum nonlocality [16,17], and the direct characterization of entanglement [18] and quantum dynamics [19]. Here we demonstrate the usefulness of hyperentanglement in metrology, allowing one to reach the ultimate quantum precision limits, for the paradigmatic case of an interaction between two degrees of freedom of the same system. Examples of this type of evolution include the interaction between spin and momentum in a Stern-Gerlach experiment, between internal and external DOF of trapped ions [20], or the polarization and spatial DOF of an optical field propagating through a birefringent medium [21]. Thus, the ideas presented here could be applied to a number of different physical scenarios and metrological tasks.

As a theoretical and experimental testbed to explore these ideas, we consider the use of hyperentangled photon pairs to monitor a tiny rotation of a mirror. We show that the entanglement in both spatial and polarization DOF leads to increased quantum advantage in metrological sensing, allowing for Heisenberg scaling in the number of photons N used to probe the rotation: the precision of estimation becomes proportional to $1/N$, instead of the shot-noise behavior $\propto 1/\sqrt{N}$. Tilt-angle estimation is important in several fields of science, involving, for instance, precision sensing of the twist angle of a torsion pendulum for the measurement of the gravitational field [22,23], the alignment of mirrors in interferometers [24], or in atomic-force microscopy [25]. A common procedure consists in detecting the spatial or phase displacement of a laser beam reflected by the mirror [26–32]. A convenient characteristic of our method is that information is retrieved solely from a binary polarization measurement. This scheme takes advantage of both hyperentanglement and beam displacement to increase the precision beyond the shot-noise limit.

Precision measurements and Fisher information. Bounds on the uncertainty in the estimation of a parameter θ can be assessed by the Cramér-Rao inequality [33]:

$$\delta\theta \geqslant \frac{1}{\sqrt{\nu F(\theta)}}, \tag{1}$$

where

$$F(\theta) = \sum_j \frac{1}{p_j(\theta)}\left[\frac{dp_j(\theta)}{d\theta}\right]^2 \tag{2}$$

is the Fisher information on θ, for a given measurement on the probe used to estimate the parameter; $p_j(\theta)$ is the probability of obtaining experimental result j, given that the value of the parameter is θ; and ν is the number of repetitions of the measurement. Maximization of $F(\theta)$ over all possible quantum measurements yields the quantum Fisher information $\mathcal{F}(\theta)$, which leads to the ultimate precision bound. Since inequality (1) can be saturated in the limit of large ν, the Fisher information can be considered as a figure of merit for the precision of a given measurement strategy. We adopt this standpoint in the following.

Hyperentanglement-enhanced tilt sensor. Figure 1 shows our experimental setup for a quantum-enhanced photonic tilt sensor based on hyperentanglement. A 325-nm He-Cd laser is used to pump two β-BaB_2O_4 (BBO) crystals (2 mm length), producing polarization and spatially entangled photon pairs via spontaneous parametric down-conversion (SPDC) [34,35] with degenerate wavelength 650 nm and propagating collinearly. The state of the twin photons is well described by $|\Psi^{(2)}\rangle = |\Phi^+\rangle \otimes |\psi^{(2)}\rangle$, where $|\psi^{(2)}\rangle$ stands for the spatial degrees of freedom of the photon pair, and $|\Phi^+\rangle = (|HH\rangle + |VV\rangle)/\sqrt{2}$ is the polarization state, with H (V) standing for

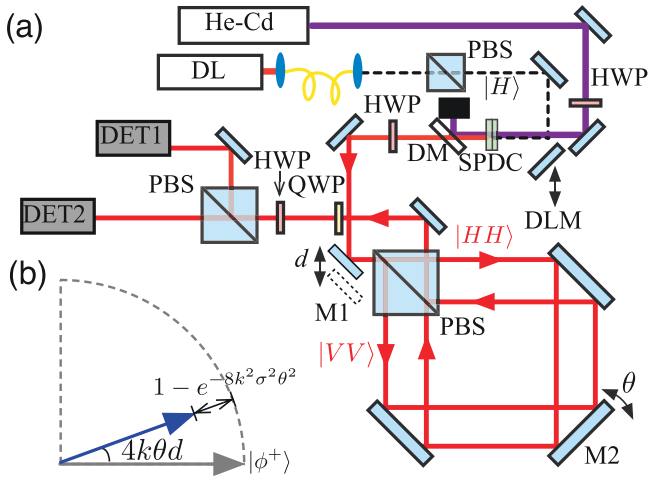

FIG. 1. (a) Experimental setup (see text). (b) One quadrant of the equatorial plane of the Bloch sphere. Tilt of mirror M2 causes the Bloch vector of the initial polarization state $|\phi^+\rangle$ to shrink and rotate.

horizontal (vertical) polarization. Within the monochromatic and paraxial approximations, the spatial state of the photon pair at the near field of the BBO source can be written as [35]

$$|\psi^{(2)}\rangle = \iint d\mathbf{q}_1 d\mathbf{q}_2 \mathcal{W}(\mathbf{q}_1+\mathbf{q}_2)\Gamma(\mathbf{q}_1-\mathbf{q}_2)|\mathbf{q}_1\rangle|\mathbf{q}_2\rangle, \quad (3)$$

where $|\mathbf{q}_1\rangle, |\mathbf{q}_2\rangle$ are transverse-position eigenstates, $\mathcal{W}$ is the Gaussian transverse spatial profile of the pump laser beam, and Γ is the phase matching function. In usual conditions, the state (3) can display a large amount of entanglement, which appears in the form of spatial correlations of the photons in the near field, and anticorrelations in the far field [35]. Moreover, these correlations can be observed simultaneously with the polarization correlations [11].

After SPDC, the pump beam is removed via a dichroic mirror (DM). Both photons are sent into a Sagnac interferometer built with a polarizing beam splitter (PBS). In this way, the H-polarized (V-polarized) photons propagate in the clockwise (counterclockwise) direction. Mirror M1 is mounted on a translation stage to adjust the initial beam displacement d. Small angular deflections θ of mirror M2 are controlled via a stepper motor and a piezoelectric actuator. To take advantage of the spatial correlations at the source plane, we use a pair of lenses (not shown) in a confocal arrangement to map the source plane onto mirror M2.

A half-wave plate (HWP) and quarter-wave plate (QWP) in conjunction with a PBS are used to project onto different polarization states. The photons are detected in coincidence, each single-photon detector equipped with an 8-mm-diameter circular aperture and a 10-nm-bandwidth filter. For measurements with independent photons, the diode laser mirror (DLM) is placed in the setup, coupling light from a 650-nm diode laser (DL) into the interferometer (He-Cd laser blocked). These photons are coupled out of a single-mode fiber (following the thin black dashed line) and aligned to follow the same propagation path as the entangled photons. They are prepared in the polarization state $|\phi^+\rangle = (|H\rangle + |V\rangle)/\sqrt{2}$ by a HWP, with the spatial state $|\psi^{(1)}\rangle$ corresponding to a Gaussian beam profile, so that the total state is $|\Psi^{(1)}\rangle = |\phi^+\rangle \otimes |\psi^{(1)}\rangle$.

When the initial beam displacement is $d = 0$, the H and V polarization components of the photons propagate collinearly in opposite directions within the interferometer. When $d \neq 0$, the two trajectories are spatially displaced in the transverse plane, as shown in the sketch of the experiment.

Tilt of mirror M2 induces transverse momentum shifts in opposite directions on the two counterpropagating beams inside the interferometer, corresponding to horizontal- and vertical-polarized components, respectively. For the initial polarization states $|\phi^+\rangle$ or $|\Phi^+\rangle$, this produces entanglement between the polarization and spatial degrees of freedom of each photon. Moreover, the tilt also induces a relative phase between the two counterpropagating beams that is proportional to the displacement d, due to the different path lengths inside the interferometer. Both of these effects can be used to retrieve information about the angle θ via monitoring the polarization state of the photons at the output of the interferometer. We consider first independent photons. For the initial state $|\phi^+\rangle$, entanglement between the two degrees of freedom leads to purity loss of the photon polarization state, which is manifested by a reduction of the length of the corresponding Bloch vector from unity to $\exp(-8k^2\sigma^2\theta^2)$, where k is the photon wave number and σ is the width of the transverse profile of the Gaussian beam at mirror M2. The relative phase between the two polarization components leads to a rotation of the Bloch vector around the z axis, by an angle $4\theta kd$. Both of these effects are illustrated in Fig. 1(b). A similar analysis applies to the two-photon state $|\Phi^+\rangle$, which behaves as an effective two-level system for this setup. However, in this case rotation and shrinking of the Bloch vector can be up to two times larger, leading to increased precision in the estimation of θ.

Heisenberg scaling via hyperentanglement. The overall effect of the interferometer on an input single-photon state can be represented by the unitary operator:

$$\hat{U}^{(1)}(\theta) = e^{-i2k\theta\hat{\sigma}_z\hat{x}}, \quad (4)$$

where $\hat{\sigma}_z = |H\rangle\langle H| - |V\rangle\langle V|$, $\hat{x}$ represents the transverse position operator, and $2k\theta$ is the shift in transverse momentum. For two photons, one has instead $\hat{U}^{(2)}(\theta) = \exp[-i2k\theta(\hat{\sigma}_{z_1}\hat{x}_1 + \hat{\sigma}_{z_2}\hat{x}_2)]$.

For a unitary evolution $\hat{U}(\theta)$ of a pure state, the quantum Fisher information $\mathcal{F}(\theta)$ is given by four times the variance in the initial state of the generator of $\hat{U}(\theta)$. From Eq. (4), the quantum Fisher information for single photons is then

$$\mathcal{F}^{(1)}(\theta) = 16k^2(\sigma^2 + d^2), \quad (5)$$

where $d = \langle\hat{x}\rangle$ is the initial transverse displacement of the beam. The term proportional to σ^2 corresponds to information on θ stemming from the momentum shift. The term proportional to d^2 arises from the relative phase between the two counterpropagating polarization components that is proportional to d, and thus depends upon the polarization coherence. The contribution d^2 increases $\mathcal{F}(\theta)$ with respect to the balanced situation $d = 0$. In particular, if $d \gg \sigma$, this can lead to a huge increase in the precision of estimation of θ. In this case, the information on θ is contained mainly in the relative phase. Although this effect has been exploited by a few authors [26,27], it is not present in most previous implementations using collinear Sagnac configurations

[28–30,32]. Furthermore, we rely in the present scheme on a simple binary polarization measurement.

The quantum Fisher information for entangled photon pairs, stemming from the corresponding unitary evolution $\hat{U}^{(2)}(\theta)$, unveils subtle effects related to not only the polarization entanglement but also spatial entanglement between the two photons. Assuming that the individual photons have the same Gaussian spatial profile with variance σ^2, one then has

$$\mathcal{F}^{(2)}(\theta) = 32k^2(\sigma^2 + \mathrm{cov}[x_1,x_2] + 2d^2), \tag{6}$$

where the covariance $\mathrm{cov}[x_1,x_2]$ corresponds to the transverse spatial correlations between the photon pairs.

There are remarkable differences between Eqs. (5) and (6). The overall multiplicative factor for photon pairs is twice that of the corresponding one for single photons, since there are two photons passing through the interferometer. The extra factor of 2 multiplying d^2 originates entirely from the polarization entanglement, which is thus seen to enhance the precision of estimation of the tilt angle. The other two terms in (6) stem from the momentum kick, which entangles the spatial and polarization DOF of each photon. If $\mathrm{cov}[x_1,x_2] = 0$, there is no gain with respect to injecting two spatially independent photons in the interferometer. On the other hand, the maximum value of the covariance is σ^2, which would correspond to perfect spatial correlation between the two photons. In this limiting case, the quantum Fisher information is maximum:

$$\mathcal{F}^{(2)}_{\mathrm{max}}(\theta) = 64k^2(\sigma^2 + d^2), \tag{7}$$

which displays a dependence with the square of the number of photons, when compared to Eq. (5). This is the well-known Heisenberg scaling for N systems: entanglement implies that the Fisher information is proportional to N^2, rather than to N, which corresponds to the shot-noise behavior (two independent photons). This enhanced scaling is due to the joint contribution of maximal spatial correlation, and to the maximal polarization entanglement. Under the same conditions, for N maximally entangled photons, we show in the Appendix that the corresponding quantum Fisher information is N^2 times $\mathcal{F}^{(1)}(\theta)$ given by Eq. (5), thus generalizing the Heisenberg scaling to more than two photons.

The quantum Fisher information $\mathcal{F}$ provides the ultimate precision limit. However, it can be challenging to find an experimentally friendly measurement strategy that allows one to reach these bounds. An advantage of the present scheme is that in the interesting limit of very small tilt angles, $(\theta k\sigma)^2 \ll 1$ and $(\theta kd)^2 \ll 1$, the quantum Fisher information can be reached via a simple binary polarization measurement: projection of the final polarization state onto the basis defined by the initial state and the one orthogonal to it.

With this polarization measurement, one can estimate the probability $p^{(\ell)}(\theta)$ to project the final polarization state onto the initial state. Applying $\hat{U}^{(\ell)}(\theta)$ to the initial state, it is straightforward to show that

$$p^{(\ell)}(\theta) = \tfrac{1}{2}\left[1 + V\cos(4\ell\theta kd)\exp\left(-8\ell\theta^2k^2\sigma^2_{(\ell)}\right)\right], \tag{8}$$

where $\ell = 1$ ($\ell = 2$) for single (entangled) photons, $\sigma^2_{(\ell)} \equiv \sigma^2 + (\ell-1)\mathrm{cov}[x_1,x_2]$, and V is the visibility of the interferometer. The probability $p^{(\ell)}(\theta)$ corresponds to an interference curve, with an additional damping term given by the Gaussian function. Information on θ can be obtained from both the oscillatory cosine term as well as the Gaussian. The corresponding Fisher information is given by

$$F^{(\ell)}(\theta) = \frac{16V^2\ell^2k^2\left[d\,\sin(4\ell\theta kd) + 4k\theta\sigma^2_{(\ell)}\cos(4\ell\theta kd)\right]^2}{\exp\left(16\ell\theta^2k^2\sigma^2_{(\ell)}\right) - V^2\cos^2(4\ell\theta kd)}. \tag{9}$$

When $(\theta k\sigma_{(\ell)})^2 \ll 1$, $(\theta kd)^2 \ll 1$, and $V = 1$, this expression coincides with (5) for $\ell = 1$ and with (6) for $\ell = 2$, up to terms of second order in $\theta k\sigma_{(\ell)}$ and θkd. Thus, within this approximation, the binary polarization measurement reaches the maximum precision limit given by the quantum Fisher information in both the single- and the two-photon case.

Experimental demonstration of quantum enhancement. Entangled photons in the state $|\Psi^{(2)}\rangle = |\Phi^+\rangle \otimes |\psi^{(2)}\rangle$ were injected into the Sagnac interferometer, and the mirror angle θ was scanned. We measured the probability $p^{(2)}(\theta)$ to project the two-photon state at the output of the interferometer onto the polarization state $|\Phi^+\rangle$, as a function of θ. For the experiment with independent photons, an attenuated laser beam, prepared in the polarization state $|\phi^+\rangle$, was injected into the interferometer. The probability $p^{(1)}(\theta)$ to detect the state $|\phi^+\rangle$ was obtained as a function of θ. In both cases, we controlled the initial displacement d of the photon beams by translating their initial positions before entrance into the interferometer using mirror M1.

Figure 2 compares experimental results for $p^{(\ell)}(\theta)$ obtained for independent photons [plots (a) and (c)] and entangled photon pairs [plots (b) and (d)] when scanning the tilt angle θ of mirror M2. The red circles and black squares are data points and the solid curves are fits using Eq. (8). Error bars were calculated from propagation of Poissionian count statistics, and are smaller than the plot symbols in most cases. From the curve fits we extract the visibility V, as well as the variances $\sigma^2_{(\ell)}$. For the variances, the fits return values $\sigma^2_{(1)} \approx 0.65 \pm 0.05$ mm^2 and $\sigma^2_{(2)} \approx 1.1$–$1.34$ mm^2, with typical uncertainty less than 0.1 mm^2. These agree with independent measurements of the single- and two-photon beams near mirror M2, obtained by scanning a thin slit aperture, giving $\sigma^2_{(1)} = 0.65 \pm 0.02$ mm^2 and $\sigma^2_{(2)} = 1.22 \pm 0.04$ mm^2. The variance of the individual beams of the photon pair at mirror M2 were both $\sigma^2 = 0.70 \pm 0.03$ mm^2. The displacement d was left as a free fit parameter, and estimates returned values comparable to the expected values. Using the values obtained from the curve fits to $p^{(\ell)}(\theta)$ we plot the corresponding Fisher information using Eq. (9), given by the blue curves, with the experimental uncertainty given by the light shaded regions.

In the plots shown in Fig. 2 one can see the damped oscillatory behavior of $p^{(\ell)}(\theta)$, where the oscillation frequency is proportional to the beam displacement d. We obtained visibilities in the range $V \approx 0.72$–0.77 ± 0.01 for the two-photon case, which is much less than the ideal case $V = 1$. This is due mostly to the relative phase variation of the polarization state along the collinear two-photon beam of photons incident on our 8-mm-diameter detection apertures [34], which are necessary to exploit the full range of spatial entanglement. The visibilities could be improved in future experiments by using thinner nonlinear crystals, narrower spectral filters, and/or additional compensation crystals [36]. This effect, along with the mode

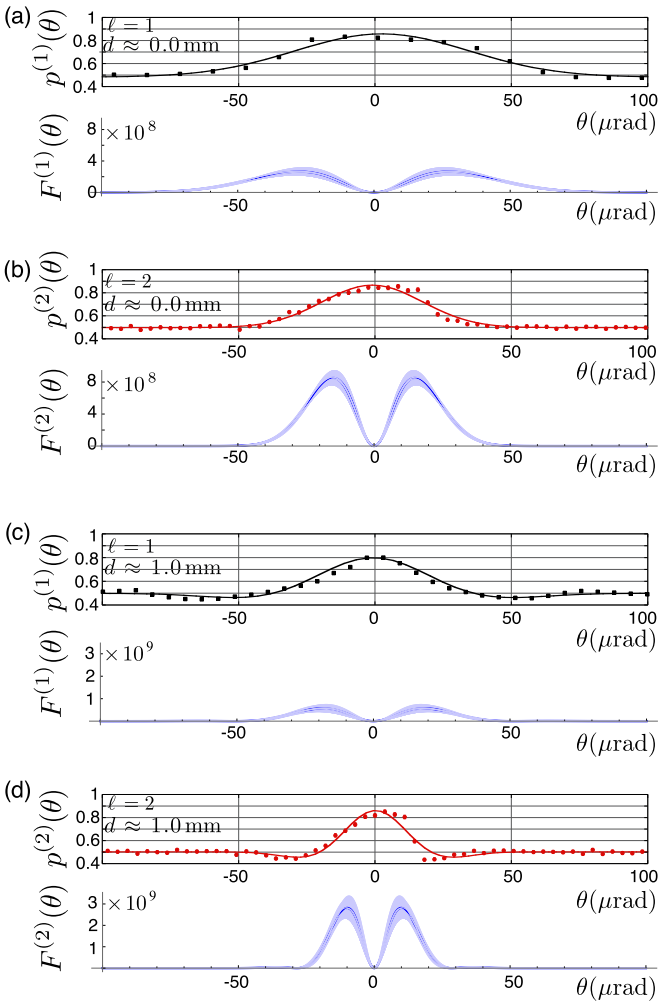

FIG. 2. Experimental probability $p^{(\ell)}(\theta)$ and corresponding Fisher Information $F^{(\ell)}(\theta)$ (blue curves) as a function of θ for different values of the initial displacement d. Black squares in (a) and (c) correspond to independent photons ($\ell = 1$), while the red circles in (b) and (d) correspond to hyperentangled photon pairs ($\ell = 2$). The red and black curves are fits to Eq. (8). From the fit parameters we plotted the theoretical curves (in blue) for the Fisher information, given by Eq. (2).

mismatch in the interferometer, contributes to produce an effective dephasing channel for the polarization state. The independent-photon experiment leads to higher visibilities. However, in order to have a direct comparison between the two cases, in the independent-photon experiment we reduce the visibility by slightly misaligning the interferometer, so as to have similar values in both situations. Comparisons of plot 2(a) with 2(b), and 2(c) with 2(d), clearly displays the quantum enhancement: the maximum Fisher information corresponding to the photon pair is approximately four times the corresponding one for single photons. This shows that hyperentanglement leads to an increase in the precision of estimation, as compared to the independent-photon situation. It is important to stress that the displacement d fulfills an important role in increasing the Fisher information in both cases: as mentioned before, displacing the beam at the input

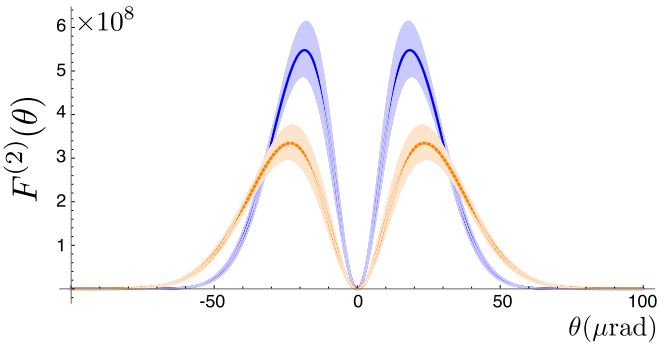

FIG. 3. Experimentally determined Fisher information $F^{(2)}(\theta)$ as a function of θ for the input state $|\Phi^+\rangle$ for different values of the initial spatial correlation, and displacement $d = 0$. The blue solid curve corresponds to larger correlation $C = 0.84 \pm 0.14$, while the orange dashed curve corresponds to $C = 0.18 \pm 0.10$ (see text).

of the interferometer is a useful resource for increasing the precision of estimation.

To show that there is indeed an increased sensitivity due to the correlations coming from spatial entanglement, we used a spatial filter to alter the spatial correlation between the photons, in such a way that the widths of the marginal distributions were kept constant. Figure 3 shows the resulting Fisher information for $d = 0$, when only the effect of the momentum kick is relevant. Let us quantify the spatial correlation using a correlation coefficient $C = \mathrm{cov}[x_1, x_2]/\sigma^2$. The blue solid curves correspond to high spatial correlation $C = 0.84 \pm 0.14$, while the orange dashed curves correspond to the case where $C = 0.18 \pm 0.10$. The plots clearly display the contribution from spatial entanglement to the Fisher information.

Even with a nonideal visibility, $V = 0.77 \pm 0.01$, it was possible to achieve sub-shot-noise precision, as displayed in Fig. 4, where $d = 5.97 \pm 0.05$ mm. The enhancement in the Fisher information for $d \gg \sigma$ is due primarily to polarization entanglement. The dashed line corresponds to the quantum Fisher information for two independent photons, which leads to the shot-noise limit in this case. It represents the maximal

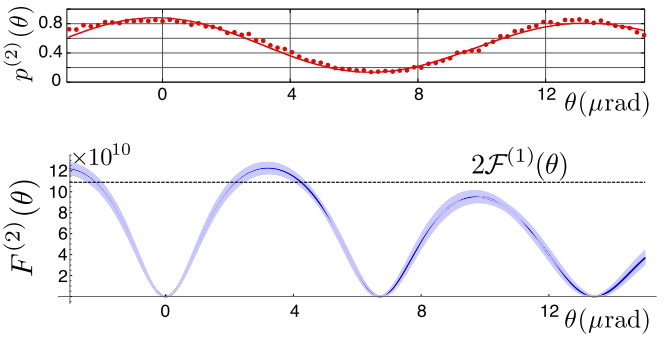

FIG. 4. Experimental probability $p^{(2)}(\phi^+)$ (red circles) and corresponding Fisher Information F_2 (blue curve) as a function of θ for $d = 6$ mm. The red curve is a fit using Eq. (8) for $\ell = 2$, which yields the detection probability for the two-photon polarization state. From the fit parameters the Fisher information is plotted, using Eq. (2). Precision beyond shot noise, given by the horizontal dashed line, is clearly displayed.

information about θ that can be retrieved by sending two independent photons into the interferometer, in the ideal situation of $V = 1$. It is also important to note that the additivity of the Fisher information implies that $N/2$ photon pairs in our scheme (N photons total) beat the shot-noise limit for N independent photons, given by $N\mathcal{F}^{(1)}(\theta)$.

We note from Figs. 2 and 4 that the sub-shot-noise regime is achieved only for larger values of d. Analyzing Eq. (9) for $d = 0$ and $d \gg \sigma$, we see that this is due to the fact that the momentum kick contribution is much more sensitive to the loss of visibility, as compared to the rotation due to the phase difference between the two counterpropagating polarization components. This last contribution becomes more important as d increases, thus mitigating the effect of visibility loss.

Summary and outlook. We have demonstrated that hyperentanglement can be an important and useful resource for quantum metrology, allowing for the attainment of Heisenberg scaling and the sub-shot-noise regime, even in the presence of experimental imperfections. Our method, when applied to optical interferometry, uses a displaced input beam to greatly boost the precision in the estimation of the tilt angle of a mirror. This allows for multiple degrees of freedom to contribute, leading to increased sensitivity even for independent photons, when compared to schemes employing collinear Sagnac configurations. Furthermore, this displacement is essential to exploit the quantum gain in sensitivity that results from polarization entanglement.

The scheme presented in this Rapid Communication is particularly simple and reliable, since it involves only a binary measurement on a two-level system. The ideas developed here have a broad range of applications, since the basic dynamics, involving the bilinear coupling between continuous and discrete bidimensional degrees of freedom, are common to many systems, such as Stern-Gerlach devices, optical birefringence, and trapped ions. Our results demonstrate yet another useful role of hyperentanglement: it is a resource for increasing the precision of metrological tasks.

Acknowledgments. The authors acknowledge financial support from the Brazilian agencies CNPq, FAPERJ, CAPES, and the National Institute of Science and Technology–Quantum Information.

APPENDIX: QUANTUM FISHER INFORMATION FOR N HYPERENTANGLED PROBE SYSTEMS

The quantum Fisher information for the estimation of the tilt angle θ, for N-partite pure states under unitary evolution is $\mathcal{F}^{(N)}(\theta) = 4\langle\Delta\hat{H}^2\rangle$, where in the present case the Hamiltonian $\hat{H}$ is given by $2k\sum_{j=1}^{N}\hat{\sigma}_{z_j}\hat{x}_j$. Consider an initial N-partite pure state, where each physical system contains one two-level degree of freedom and one continuous degree of freedom. Let the N-partite hyperentangled state be $|S\rangle = |\Phi\rangle \otimes |\psi\rangle$, where $|\Phi\rangle = (|0\rangle^{\otimes N} + |1\rangle^{\otimes N})/\sqrt{2}$ is a Greenberger–Horne–Zeilinger (GHZ) state of N qubits and $|\psi\rangle$ refers to a state of N quantum continuous variables. Assuming, as was done in relation to Eq. (6) of the main text, that for each system we have $\langle\Delta\hat{x}_j\rangle = \sigma^2$, and $\langle\hat{x}_j\rangle = d$, it is straightforward to show that

$$\mathcal{F}^{(N)}(\theta) = 16k^2\left(N\sigma^2 + N^2d^2 + 2\sum_{j=1}^{N}\sum_{i=1}^{j-1}\mathrm{cov}[x_i,x_j]\right), \tag{A1}$$

where we used the fact that $\langle\hat{\sigma}_{z_j}\rangle = 0$ and $\langle\hat{\sigma}_{z_j}\hat{\sigma}_{z_i}\rangle = 1$. Equation (A1) generalizes Eq. (6) of the text. In the limit in which the covariances attain their maximum value, equal to σ^2, one has

$$\mathcal{F}^{(N)}_{\max}(\theta) = N^2 16k^2(\sigma^2 + d^2) = N^2\mathcal{F}^{(1)}(\theta), \tag{A2}$$

which clearly displays Heisenberg scaling.

In our experiment, $N = 2$, $|\psi^{(2)}\rangle$ refers to the spatial degrees of freedom of twin photons, given by Eq. (3), while $|\Phi\rangle = |\Phi^+\rangle$ is a maximally entangled polarization state. In this case, Eq. (A1) leads to Eq. (6), and Eq. (A2) to Eq. (7).

[1] J. J. Bollinger, W. M. Itano, D. J. Wineland, and D. J. Heinzen, Optimal frequency measurements with maximally correlated states, Phys. Rev. A **54**, R4649 (1996).
[2] H. Lee, P. Kok, and J. P. Dowling, A quantum Rosetta stone for interferometry, J. Mod. Opt. **49**, 2325 (2002).
[3] V. Giovannetti, S. Lloyd, and L. Maccone, Quantum-enhanced measurements: Beating the standard quantum limit, Science **306**, 1330 (2004).
[4] V. Giovannetti, S. Lloyd, and L. Maccone, Quantum Metrology, Phys. Rev. Lett. **96**, 010401 (2006).
[5] L. Aolita, R. Chaves, D. Cavalcanti, A. Acín, and L. Davidovich, Scaling Laws for the Decay of Multiqubit Entanglement, Phys. Rev. Lett. **100**, 080501 (2008).
[6] M. Kacprowicz, R. Demkowicz-Dobrzański, W. Wasilewski, K. Banaszek, and I. A. Walmsley, Experimental quantum-enhanced estimation of a lossy phase shift, Nat. Photonics **4**, 357 (2010).
[7] L. Aolita, F. de Melo, and L. Davidovich, Open-system dynamics of entanglement: A key issues review, Rep. Prog. Phys. **78**, 042001 (2015).
[8] P. G. Kwiat, Hyper-entangled states, J. Mod. Opt. **44**, 2173 (1997).
[9] P. G. Kwiat and H. Weinfurter, Embedded Bell-state analysis, Phys. Rev. A **58**, R2623 (1998).
[10] S. P. Walborn, S. Pádua, and C. H. Monken, Hyperentanglement-assisted Bell-state analysis, Phys. Rev. A **68**, 042313 (2003).
[11] M. P. Almeida, S. P. Walborn, and P. H. S. Ribeiro, Simultaneous observation of correlations in position-momentum and polarization variables, Phys. Rev. A **73**, 040301(R) (2006).
[12] J. T. Barreiro, T.-C. Wei, and P. G. Kwiat, Beating the channel capacity limit for linear photonic superdense coding, Nat. Phys. **4**, 282 (2008).
[13] T. M. Graham, H. J. Bernstein, M. J. T.-C. Wei, and P. G. Kwiat, Superdense teleportation using hyperentangled photons, Nat. Commun. **6**, 7185 (2015).
[14] S. P. Walborn, M. P. Almeida, P. H. S. Ribeiro, and C. H. Monken, Quantum information processing with hyperentangled photon states, Quantum Inf. Comput. **6**, 336 (2006).

[15] G. Vallone, G. Donati, R. Ceccarelli, and P. Mataloni, Six-qubit two-photon hyperentangled cluster states: Characterization and application to quantum computation, Phys. Rev. A **81**, 052301 (2010).

[16] C. Cinelli, M. Barbieri, R. Perris, P. Mataloni, and F. De Martini, All-Versus-Nothing Nonlocality Test of Quantum Mechanics by Two-Photon Hyperentanglement, Phys. Rev. Lett. **95**, 240405 (2005).

[17] M. Barbieri, F. De Martini, P. Mataloni, G. Vallone, and A. Cabello, Enhancing the Violation of the Einstein-Podolsky-Rosen Local Realism by Quantum Hyperentanglement, Phys. Rev. Lett. **97**, 140407 (2006).

[18] S. P. Walborn, P. H. S. Ribeiro, L. Davidovich, F. Mintert, and A. Buchleitner, Experimental determination of entanglement with a single measurement, Nature (London) **440**, 1022 (2006).

[19] T. M. Graham, J. T. Barreiro, M. Mohseni, and P. G. Kwiat, Hyperentanglement-Enabled Direct Characterization of Quantum Dynamics, Phys. Rev. Lett. **110**, 060404 (2013).

[20] D. Leibfried, R. Blatt, C. Monroe, and D. Wineland, Quantum dynamics of single trapped ions, Rev. Mod. Phys. **75**, 281 (2003).

[21] N. W. M. Ritchie, J. G. Story, and R. G. Hulet, Realization of a Measurement of a "Weak Value", Phys. Rev. Lett. **66**, 1107 (1991).

[22] O. V. Karagioz, A. H. Silin, and V. P. Izmaylov, On the relation between the constant of gravitation and the distance between the interacting masses, Izv. Acad. Sci. USSR, Phys. Solid Earth **17**, 66 (1981).

[23] G. T. Gillies, The Newtonian gravitational constant: recent measurements and related studies, Rep. Prog. Phys. **60**, 151 (1997).

[24] V. Collaboration, The commissioning of the central interferometer of the Virgo gravitational wave detector, Astropart. Phys. **21**, 1 (2004).

[25] S. Alexander, L. Hellemans, O. Marti, J. Scheneir, V. Elings, P. K. Hansma, M. Longmire, and J. Gurley, An atomic-resolution atomic-force microscope implemented using an optical lever, J. Appl. Phys. **65**, 164 (1989).

[26] J. G. Park and K. Cho, High-precision tilt sensor using a folded Mach–Zehnder geometry in-phase and quadrature interferometer, Appl. Opt. **55**, 2155 (2016).

[27] J. Martínez-Rincón, C. A. Mullarkey, G. I. Viza, W.-T. Liu, and J. C. Howell, Ultrasensitive inverse weak-value tilt meter, Optics Lett. **42**, 2479 (2017).

[28] D. J. Starling, P. B. Dixon, A. N. Jordan, and J. C. Howell, Optimizing the signal-to-noise ratio of a beam-deflection measurement with interferometric weak values, Phys. Rev. A **80**, 041803 (2009).

[29] G. B. Alves, B. M. Escher, R. L. de M. Filho, N. Zagury, and L. Davidovich, Weak-value amplification as an optimal metrological protocol, Phys. Rev. A **91**, 062107 (2015).

[30] J. Martínez-Rincón, W.-T. Liu, G. I. Viza, and J. C. Howell, Can Anomalous Amplification be Attained without Postselection?, Phys. Rev. Lett. **116**, 100803 (2016).

[31] K. Lyons, S. Pang, P. G. Kwiat, and A. N. Jordan, Precision optical displacement measurements using biphotons, Phys. Rev. A **93**, 043841 (2016).

[32] G. B. Alves, A. Pimentel, M. Hor-Meyll, S. P. Walborn, L. Davidovich, and R. L. de M. Filho, Achieving metrological precision limits through postselection, Phys. Rev. A **95**, 012104 (2017).

[33] H. Cramér, *Mathematical Methods of Statistics* (Princeton University, Princeton, 1946).

[34] P. G. Kwiat, E. Waks, A. G. White, I. Appelbaum, and P. H. Eberhard, Ultrabright source of polarization-entangled photons, Phys. Rev. A **60**, R773 (1999).

[35] S. P. Walborn, C. H. Monken, S. Pádua, and P. H. S. Ribeiro, Spatial correlations in parametric down-conversion, Phys. Rep. **495**, 87 (2010).

[36] J. B. Altepeter, E. R. Jefferey, and P. G. Kwiat, Phase-compensated ultra-bright source of entangled photons, Opt. Express **13**, 8951 (2005).